COMPDYN 2019
7th ECCOMAS Thematic Conference on
Computational Methods in Structural Dynamics and Earthquake Engineering
M. Papadrakakis, M. Fragiadakis (eds.)
Crete, Greece, 24–26 June 2019

EXPERIMENTAL TESTS ON STEEL PLATES WITH CFRP STRENGTHENING

Konstantinos Vlachakis, Sofia Vlachaki-Karagiannopoulou and Ioannis Vayas

Institute of Steel Structures, National Technical University of Athens, Greece
e-mail: kostasvlachakis@yahoo.gr, sophia.vlachaki@gmail.com, vastahl@central.ntua.gr

Abstract

The application of Fiber Reinforced Polymer (FRP) strips is common for rehabilitation and strengthening of concrete structures. Still, the strengthening of steel profiles with FRPs has received little attention so far. In this direction, three tests were performed on steel plates strengthened with Carbon Fiber Reinforced Polymers (CFRP) at the Institute of Steel Structures, NTUA. They comprised one tensile and two four-point bending tests on composite specimens that consisted of one 3mm thick steel plate and one 1.2mm thick CFRP plate bonded together in order to make a preliminary estimation of the CFRP strengthening effect. The first four-point bending test was performed with the CFRP on the tension side, while the second test employed the CFRP on the compression side of the specimen. Analytical approaches as well as numerical nonlinear analyses using finite elements were employed to gain intuition and further substantiate the results. In conclusion, CFRP strengthening was found to be an effective strengthening method, which enhances ductility, tensile and bending capacity of the steel plate by almost five times, regardless of whether the CFRP is used under tension or compression. Notably, the CFRP plates, despite their slenderness were found to offer considerable resistance to compression stresses.

Keywords: Experimental tests, Carbon Fiber Reinforced Polymers (CFRP), Steel strengthening, numerical analyses, analytical procedure.

1 INTRODUCTION

The application of fiber-reinforced polymers (FRP) has been long established in teaching, research, design and regulation for strengthening and repair of concrete structures [1] – [4]. However, such an activity for steel structures is relatively new although strengthening of steel structures by means of FRPs has gained attention in recent times [5]. The main application fields refer to enhancing the moment capacity of steel or composite girders in building/bridge applications [6], [7], increasing the local buckling resistance of thin-walled compression elements [8], repair through crack-patching of fatigue prone details [9], or increase strength and ductility by means of confinement of steel or concrete filled steel tubes [10], [11]. It is therefore not surprising that, at least in Europe, there is a lack of regulations on the subject, except probably an Italian guideline [12], while the European seismic code for assessment and retrofitting of buildings [2] provides information for FRP-interventions in reinforced concrete structures only and not for steel or composite structures.

The potential for structural interventions in steel structures by means of FRPs is high, at least in some areas, despite the fact that conventional interventions with steel for steel structures are easier to implement than with concrete for concrete structures. Indeed, it is simpler to remove and repair damaged steel parts or entire structural members and easier to attach for strengthening purposes new to existing steel through welding or bolting, than remove, repair or strengthen through jacketing existing concrete members. An area where FRP composites might be applied with big advantages is for strengthening of masts and towers, like for telecommunication towers that are often in need of strengthening due to their occupation with more and larger antennas. Indeed, the classical method for strengthening tower legs where a second angle profile is added in a star battened configuration may be substituted by adhesive bonding of FRP plates to the existing angle profile. This leads to a smaller attack area of the strengthened member for the wind and a smaller periphery for the snow loading, leading to increased resistance and less loading, while the conventional method leads to increased resistance and higher loading. In addition, the operation could be handled easier due to less weight to be lifted, less space needed and, probably, lower susceptibility to environmental influences. Another area of potential beneficial application is for buildings in seismic areas where FRP plates could be attached to the beam flanges near the beam-to-column joints, in order to move the plastic hinges away from the joints, or added panel zones to increase their shear capacity. The interest for such research at European level appears to attract attention and is funded by the Research Fund for Coal and Steel (RFCS) in the ANGELHY project [13] and the German Academic Exchange Service (DAAD) in a project of hybrid strengthening methods [14].

Characteristic for these applications is that FRP composites are added in both tension and compression zones of elements, as well as in zones subjected to both compression and tension. Indeed, tower legs or bracing members may be subjected to compression or tension forces depending on the wind direction, flanges of beams in building frames in seismic areas are subjected alternatively to compression and tension, depending on the direction of the seismic excitation and the same happens to the applied shear forces of panel zones.

Design for FRP strengthening of steel elements is currently based on the nominal FRP material properties as supplied by the fabricators. These material properties, such as modulus of elasticity, tensile strength or elongation at fracture, refer exclusively to tension. Indeed, international test specifications for FRP material refer only to tensile testing, [15] to [18], obviously due to the fact that FRP material is predominantly used for tension and too thin to be directly tested for compression. The tension properties are also used, unchanged, in analytical formulae proposals for the prediction of the global or local buckling resistance of compression

members [8]. However, this approach may be questioned due to the fact that the compression resistance of FRPs is expected to be lower than the resistance to tension. It would be therefore beneficial to test the material under compression and check whether the compression properties are the same as for tension. Unfortunately, there is no international specification providing a test method, but for such a test the FRP material should be obviously attached to another element from the material that is intended to strengthen. Another issue, unspecified yet, is whether compression originates in the test from axial force or bending. For the current research it was accordingly considered necessary to investigate prior to the full-scale tests on angle leg columns, complete towers or beam-to-column joints, as planned in the relevant projects, the compression and tension behavior of FRP stripes bonded to steel plates. This would help the determination of the relevant properties and the correct design of the interventions.

This paper presents experimental, analytical and numerical investigations on the behavior of composite steel-CFRP specimens subjected to a tension and two four-point bending tests, one with the CFRP material on the tension side, the other on the compression side. The purpose was to determine the properties of FRP plates in tension separately from whether the tension arises from external axial forces or bending moments, and in compression arising from bending moments. Carbon fiber-reinforced polymer (CFRP) was used as composite material due to its high elastic modulus and tensile strength. The research was carried out in the frame of the MSc-Theses of the two first authors [19], [20].

2 GENERAL SPECIFICATIONS

The test specimens were constructed by the partner of the DAAD project [14] at the Brandenburg University of Technology (BTU) in Germany. They had the same dimensions and were made by the same materials. Each one was consisted by two parts, a 3mm thick steel plate with dimensions 80x250mm and a 1.2mm thick CFRP plate with the same dimensions (80x250mm). The two parts were bonded with a structural adhesive along their whole surface, with measured thicknesses of 1.3, 1.1 and 1.1 mm for the specimens 1, 2 and 3 respectively. Two aluminum tabs with dimensions 84x100x3mm were also used at the specimen's ends on the side of the CFRP plate, in order to protect the fibers and avoid a local failure or a fibers' break at the sections that are attached in the machine's grips in the tensile test or at the points of load application in bending tests. The side and plan view of the specimens are shown in Fig. 1, while Fig. 2 shows pictures of the specimens before testing.

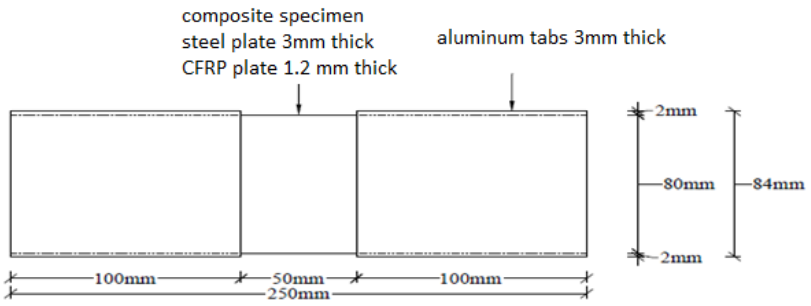

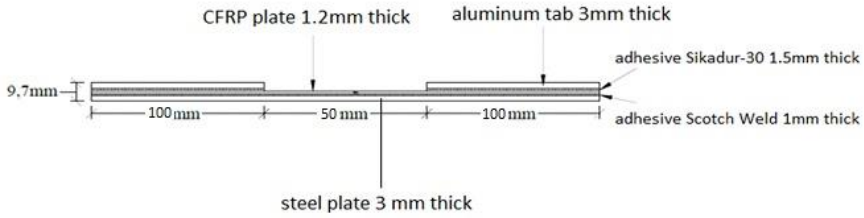

Figure 1: Plan and side view of the specimens

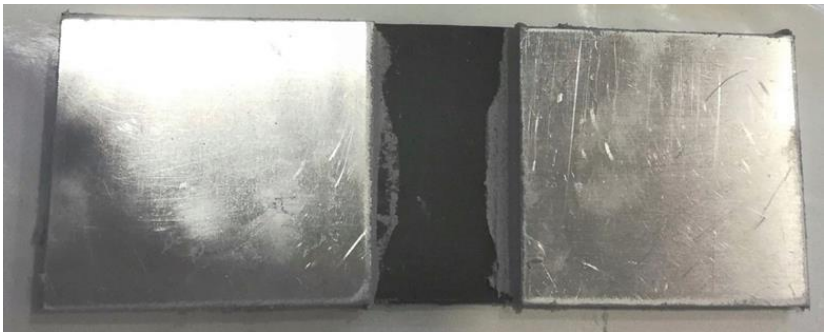

Figure 2: Picture of the specimen before testing

The mechanical properties of the constituent materials have been determined experimentally by tensile testing, carried out in an INSTRON 300XL universal machine with 300kN capacity. Steel has been tested by two tests in accordance with [21]. The resulting σ-ε-curve is shown in Fig. 3, the mechanical properties, as average from the two tests, in Table 1.

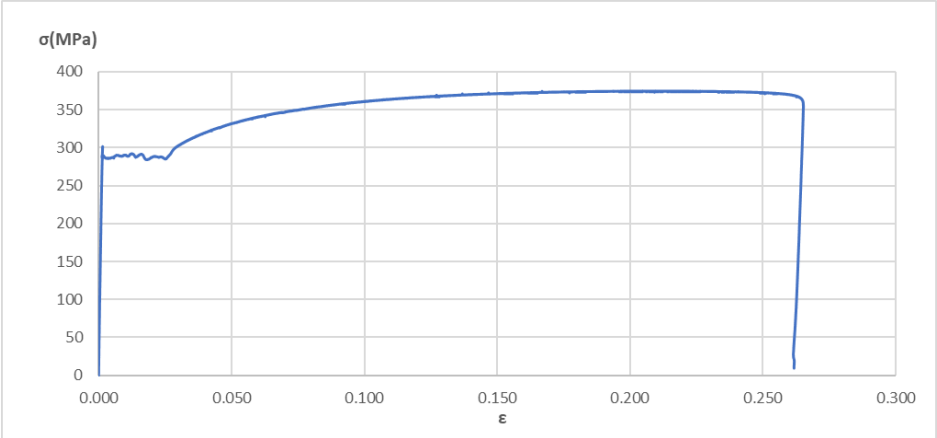

Figure 3: Experimental stress-strain curve for steel

E (MPa)	Yield stress σ_y (MPa)	Yield strain ε_y (%)	Hardening stress σ_R (MPa)	Hardening strain ε_R (%)	Ultimate stress σ_{max} (MPa)	Ultimate strain ε_{max} (%)
210000	287.5	0.1364	291	2.886	375	39.818

Table 1: Material properties of steel

The CFRP plates were made by MC Brauchemie and are considered as “low strength” plates. Their designation is 160/2400, i.e. the nominal modulus of elasticity is 160 GPa and the ultimate strength 2400 MPa. The plates were made using unidirectional fibers along the longitudinal axis of the plate. The actual mechanical properties have been determined by tensile tests on seven (7) specimens according to EN ISO 527-4 [16] and ASTM D638 -03 [17], D3039 [18]. The dimensions of the specimens were 300x25x1.5 mm, with their ends protected from the jaws of the machine by aluminum end tabs of dimensions 105x30x3 mm, as proposed by [16]. The loading speed was 1mm/min, lower than as specified in [16], in order to allow taking pictures by a thermic camera Flir B360 that was used to investigate if temperature changes take place in the material during the loading process. Strains were measured by both extensometer and strain gage. The material behaved linear elastic up to failure which was brittle and was due to the breakage of the carbon fibers, Fig. 4. Fig. 5 shows the resulting σ-ε-curves as derived from the extensometer and the strain gage measurements. The former indicates that slippage occurs between the extensometer and the specimen distorting the results. Accordingly, mechanical properties were determined on the basis of the strain gage measurements. The modulus of elasticity was determined by two methods: (a) as the slope of the curve between two predefined points with strains ε1 = 0,05% and ε2 = 0,25% proposed in [16] and (b) as the linear trendline of the σ-ε-curve from the origin up to failure. The average value from the tests was for method (a) ≈130 GPa, while for method (b) ≈141 GPa. Both methods delivered lower value than the nominal value provided by the producer, possibly due to the fact that only one strain gage was used on one side of the specimen so that effects of eccentricity were present. The average values for the ultimate stress was 2734 MPa, i.e. higher than the nominal value, as expected, and for the ultimate strain 1.91%.

Figure 4: CFRP specimens at failure

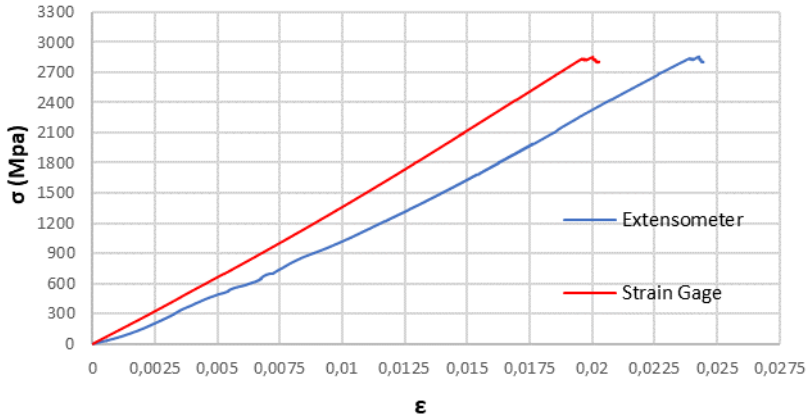

Figure 5: Experimental stress-strain curve for CFRP

The structural epoxy resin Scotch WeldTM DP 490 was used as adhesive to bond steel and CFRP plate, which is characterized by its simple and easy application and therefore recommended by its producer as appropriate for steel sections. Its ultimate shear stress τ_k and normal stress σ_k are estimated based on [5] and are shown in Table 2.

E_k (MPa)	Shear strength τ_k (MPa)	Shear modulus G_k (MPa)
3036	3.76	308.9

Table 2: Material properties of adhesive, average values

This adhesive was not strong enough to bond the aluminium tabs at the specimen's ends to the CFRP plates, so that Sikadur 30 from SIKA with nominal shear strength of 20 MPa was used instead.

As mentioned before, the specimens were fabricated at the Brandenburg University of Technology, Germany, following a specific procedure. Firstly, a special treatment using a hard brush was implemented to the steel surface, to increase the surface roughness in order to have better application of the adhesive. Then the surfaces of both steel and CFRP plates were cleaned with acetone. The adhesive was added using a special equipment, Fig. 6, to allow a uniform application of the adhesive with a thickness of approximately 0.2mm over the entire surface. For this purpose, small beads with diameter 0.105-0.20 mm made from glass were placed between the two surfaces as seen in Fig. 6. The two bonded plates remained under constant pressure for seven days until the adhesive reached its total strength. However, after this procedure the adhesive's thickness was measured, as well as possible, and was estimated to be 1.3, 1.1 and 1.1 mm for specimens 1,2, and 3 respectively.

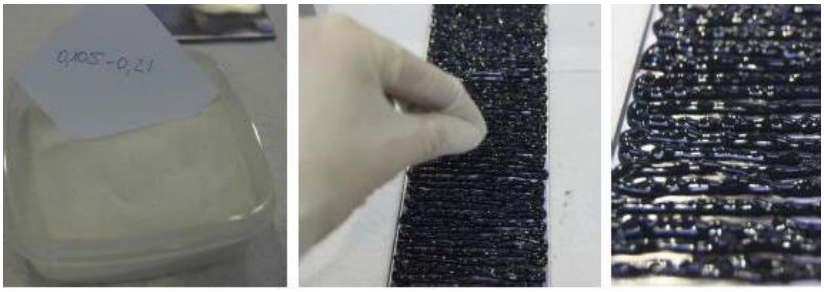

Figure 6: Application of the adhesive using special equipment

Subsequently, two aluminum tabs were also bonded on the CFRP side to protect it from the jaws of the machine. A different adhesive, Sikadur 30, was used to bond the aluminum plates to the CFRP plate**.** After that the three specimens remained seven more days under some heating lamps at a constant temperature of 33-36ºC, so that adhesive reaches its maximum strength.

3 TENSILE TEST

The tension test was carried out in the INSTRON 300XL machine. The specimen was loaded via displacement control at a testing speed of 0.2 mm/min, up to the maximum load capacity of the test machine, 300 kN, which is lower than its nominal failure load. Besides the load and the total elongation measured by the machine, strains on both the steel and the CFRP were measured by two strain gauges. The test set-up is shown in Fig. 7.

Figure 7: Test set-up for the tension test

The experimental force – displacement curve is shown in Fig. 8. The applied force is divided between the steel and the CFRP plates as in Fig. 9. It may be seen that steel behaves in the elastic-plastic, while CFRP purely in the elastic range. The force is distributed according to the stiffness of the constitutive parts as long as steel behaves elastic. When steel enters into the plastic region, it transfers only its yield force the other part transferred by the CFRP. This is because steel did not enter into the strain hardening region, as the strains measurements showed.

Assuming uniform strain distribution in the two materials, i.e. both materials are subjected to pure tension, the total force may be determined analytically and expressed by equations (1)

and (2). This assumption, which will be checked later, leads to acceptable results. This is shown in Fig. 8 where the simplified analytical curve is compared to the experimental curve.

$\varepsilon_s \leq \varepsilon_y$: $$P_{an} = E_s \cdot \varepsilon_s \cdot A_s + E_{cfrp} \cdot \varepsilon_{cfrp} \cdot A_{cfrp} \quad (1)$$

$\varepsilon_s > \varepsilon_y$: $$P_{an} = f_y + E_{cfrp} \cdot \varepsilon_{cfrp} \cdot A_{cfrp} \quad (2)$$

where:
E_s , E_{cfrp} are the modulus of elasticity of steel or correspondingly CFRP
ε_s, ε_{cfrp} are the, measured, strains of steel or correspondingly CFRP
A_s , A_{cfrp} are the cross-section areas of steel or correspondingly CFRP
ε_y, f_y are the actual yield strain and yield stress of steel

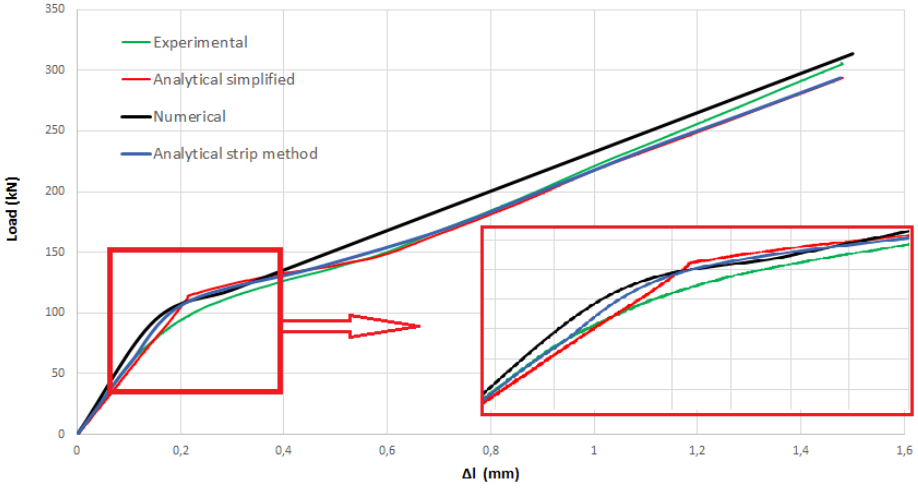

Figure 8: Experimental, analytical and numerical force – displacement curve

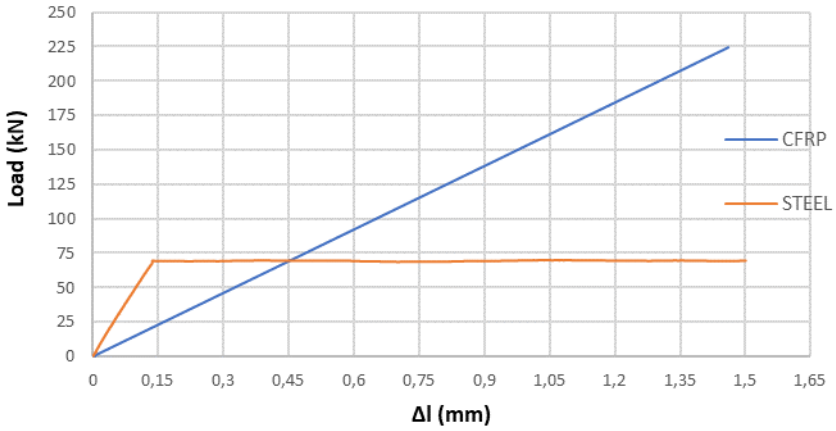

Figure 9: Partial forces transferred by the steel and CFRP plates

The specimen didn't reach failure at maximum load due to the limited capacity of the machine. However, the specimen exhibited a large permanent bow deformation after unloading as shown in Fig. 10, due to the fact that steel entered into the plastic range and exhibited a permanent tensile deformation. The corresponding plastic strain at unloading was measured by the strain gages as ε_{per} = 1,3%. This value is confirmed by appropriate geometrical measurements after the test and application of eq. (3).

$$\varepsilon_{perm} = \frac{1}{1-\frac{1}{\left(\frac{L/2}{f}\right)^2+1}} - 1 \quad (3)$$

where, Fig. 10:
f is the, measured, sagitta of the chord and
L is the, measured, chord length of the specimen.

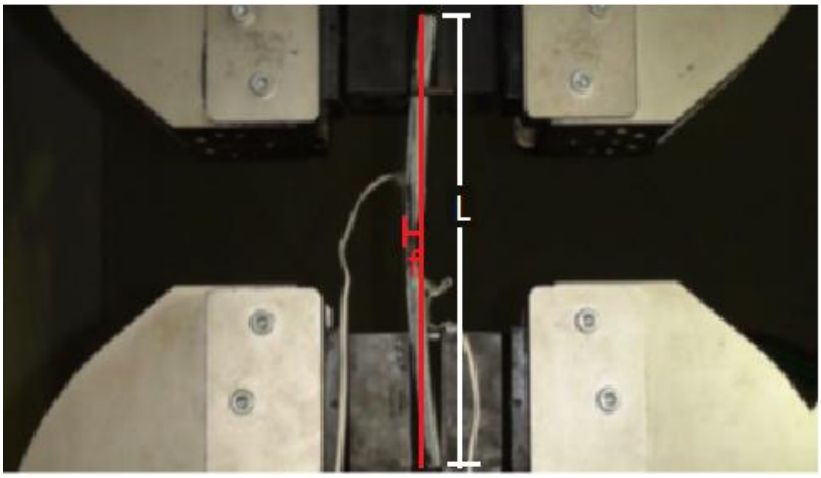

Figure 10: Permanent bow deformation after unloading. Steel on the tension (convex) side

The tension test was in addition investigated numerically using the ABAQUS Code [22]. Steel was modelled by application of solid elements of type C3D8R (Continuum solid element, 8-node linear brick, Reduced integration with hourglass control), while CFRP with shell elements of type S4R (Shell, 4-node double curved thick shell). The thickness of the shell was determined through the *Composite Layup*, by entering the number of carbon layers from which the CFRP is composed. Such a model is necessary when the orientation of the individual layers differs. In our case the same result could be achieved by a single layer with the total thickness. The end tabs and the epoxy resin were not included in the model. The interaction between steel and CFRP was introduced by connection of the two contact surfaces by means of tie constraints so that the two parts are rigidly connected with no slip between them.

The material properties of steel were introduced to follow the measured σ-ε-curve shown in Fig. 3. For the composite material the material properties were given separately for the fibers, type Graphite IM6 with modulus of elasticity E_f = 275.6 GPA, Poisson's ratio v = 0.2, ratio v_f = 51% and the matrix, type Epoxy 9310/9360 with E_m = 3.12 GPA, v_m = 0.38 and ratio v_m = 49%. The modulus of elasticity of the composite material in the longitudinal, 1, transverse, 2, and through thickness, 3, direction and the shear moduli are determined from eqs. (4) to (8) correspondingly [23]:

$$E_1 = E_f \cdot v_f + E_m \cdot v_m \quad (4)$$

$$E_2 = \frac{E_f \cdot E_m}{E_f \cdot v_f + E_m \cdot v_m} \quad (5)$$

$$E_3 = E_m \quad (6)$$

$$G_{12} = G_{13} = \frac{G_f \cdot G_m}{G_m \cdot v_f + G_f \cdot v_m} \quad (7)$$

$$G_{23} = G_m \quad (8)$$

where:

v_f, v_m are the fibers ratio and the matrix ration correspondingly and
$G = E / [2 \cdot (1+\nu)]$ for the fibers, f, and the matrix, m.
The Poisson's ratio of the composite material may be determined from:

$$\nu_{12} = \nu_{13} = \nu_f \cdot \nu_f + \nu_m \cdot \nu_m \quad (9)$$

$$\nu_{23} = \nu_m \quad (10)$$

The numerical model included the specimen over its entire length, but at the end regions where the jaws are acting the relevant displacements were restrained so that one end is fixed and the other can move freely in direction of the load application. The force – displacement curve of the numerical model is illustrated in Fig. 8, together with the experimental and analytical curves. The comparison shows a quite good agreement with the experimental and analytical results, indicating that the adopted input material parameters and the assumption of no slip between the two materials are acceptable.

However, the numerical model allows the determination of the strain and stress state separately in the two material as shown in Fig. 11 and 12. It may be seen that the stresses, and strains, at the external and internal surfaces of steel are not identical. Strains therefore vary through the specimen's thickness as shown in Fig. 13. The actual strains measured during the test were ε_{so} and ε_{cfrp} at the specimen's surface, which are similar but not identical to the strains at the centroids of the corresponding materials. The corresponding stress distribution gives rise to an internal moment that was calculated analytically by the strip method and numerically with ABAQUS and is shown in Fig. 14. This moment is in equilibrium with the external moment, calculated as the product between the applied force and the eccentricity between this force and the centroid of the composite section, calculated from eq. (11). The external moment is also illustrated in Fig. 14. There is a discrepancy between the curves of the external and internal moment that is due to the approximations made in the calculations of both. More specifically, the calculations for the internal moment assume pure axial tension with no moment in the initial loading steps, while moments arise later due to plasticity. On the other side, the external moment starts to develop from the beginning and is affine to the applied force since the eccentricity is considered unchanged during the test.

Besides the moment, the strip method was applied to calculate the axial force by integration of the axial forces in the individual strips. The relevant analytical curve is shown in Fig. 8. The comparison with the experimental curve indicates that the strip method is more accurate to the simplified one in the elastic region, while the two converge at larger strains in the plastic region of steel.

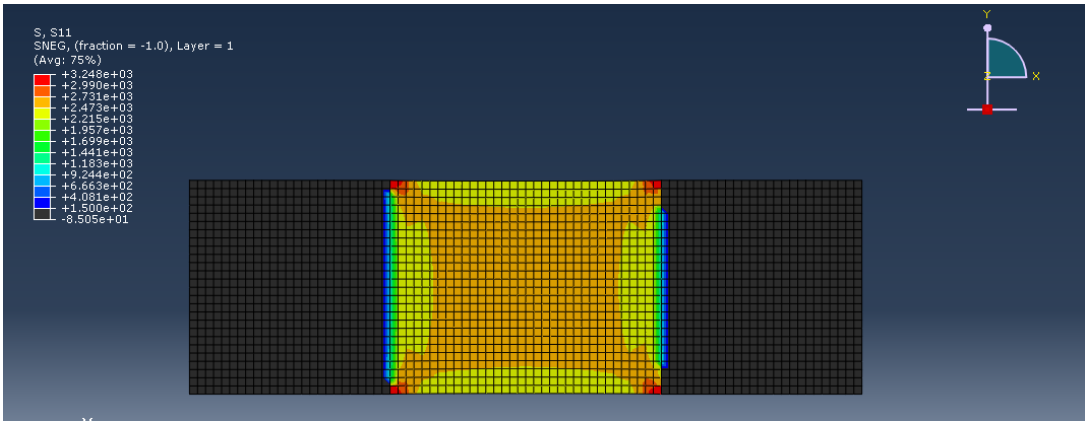

Figure 11: Stress distribution in the CFRP plate

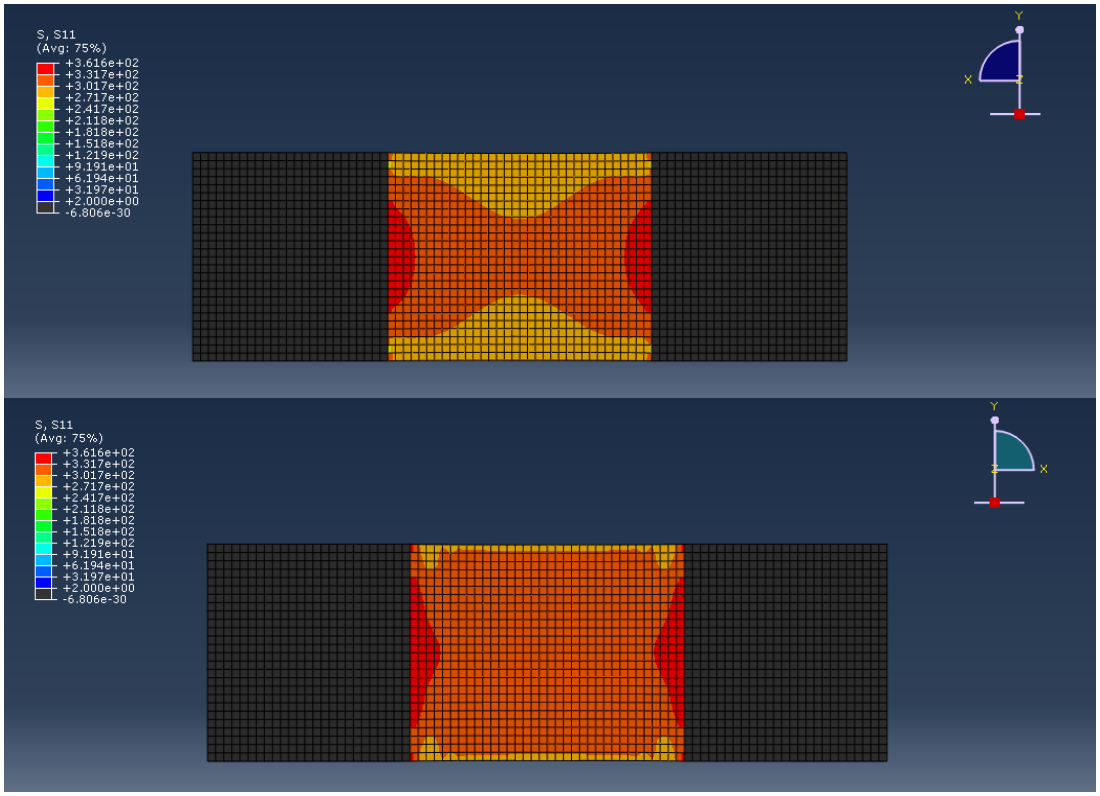

Figure 12: Stress distribution in the external and internal face of steel

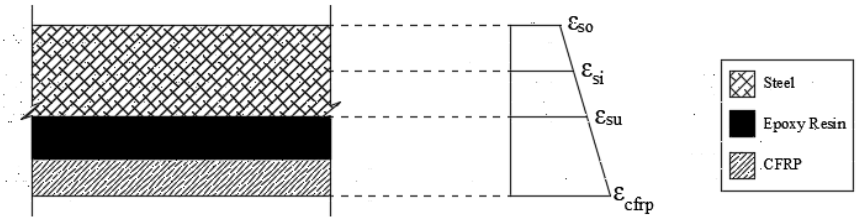

Figure 13: Actual strain distribution in the composite specimen

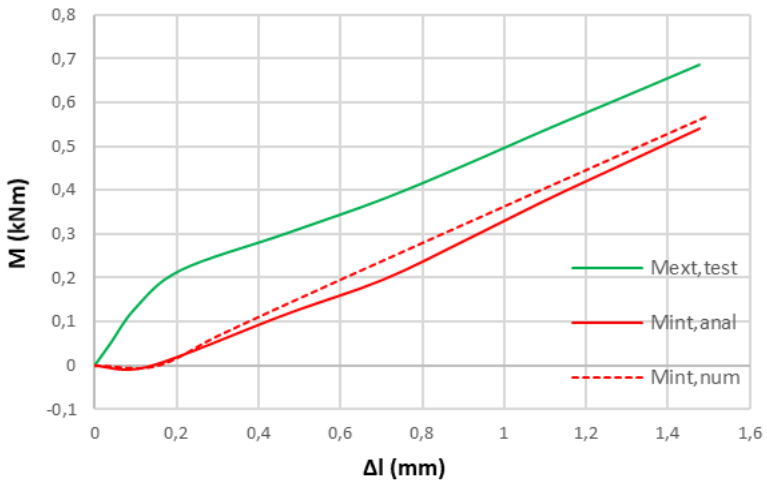

Figure 14: Moment – displacement curve of the specimen

4 FOUR-POINT BENDING TEST – FRP ON THE TENSION SIDE

The test set-up for the 4-point bending test, which was carried out in the INSTRON 300XL machine, is shown in Fig. 15. The specimen was loaded via displacement control at a testing speed of 0.42 mm/min. The recordings included the applied load, the deflection at mid-span, both measured from the machine recordings, and the strains of the steel and the FRP-plate at midspan, measured by two strain gauges. At late loading stages no steel's strain data were available because the strain gauge at the compression side was disconnected due to very high strains. Small slips also occurred at certain times during the test.

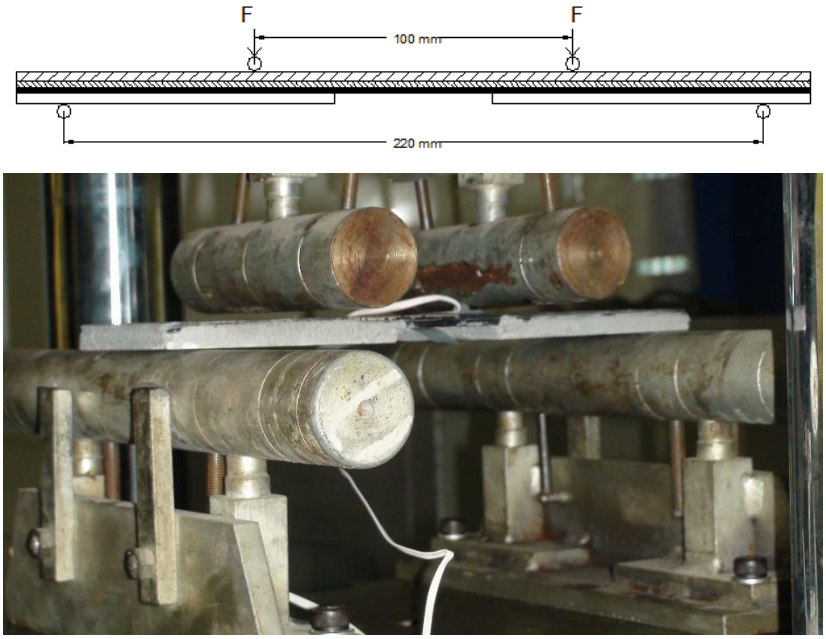

Figure 15: Test set-up for the 4-point bending test – CFRP in tension

The experimental force – deflection curve is shown in Fig. 16. At some points the load drops indicating small slips between the specimen and the supports. The experimental test was accompanied by analytical and numerical calculations. For the former two methods were adopted.

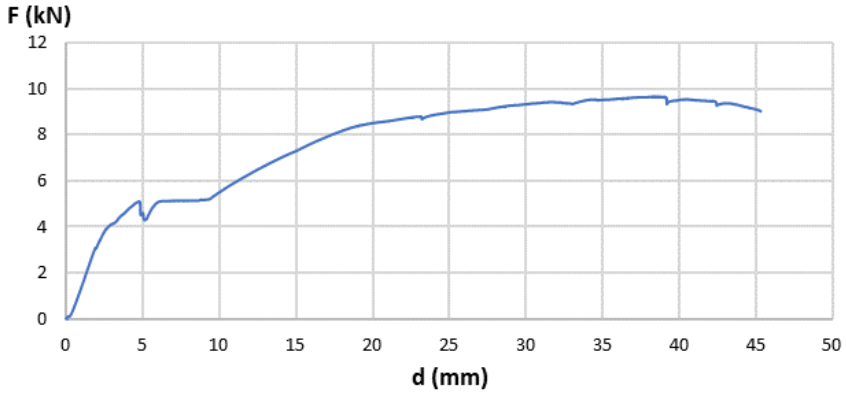

Figure 16: Experimental force – mid-span deflection curve

- Analytical Method 1

This is based on the Bernoulli-Euler beam theory for linear strain distribution over the cross section, Fig. 17. The centroid of the cross section, distance from the top side, is calculated from eq. (11):

$$zc = \frac{zs*As+(z_{res}*\frac{A_{res}}{n_{res}})+(z_{CFRP}*\frac{A_{CFRP}}{n_{CFRP}})}{As+\frac{A_{res}}{n_{res}}+\frac{A_{CFRP}}{n_{CFRP}}} \quad (11)$$

where:
z_s, z_{res}, z_{cfrp} are the centroids of steel, resin or CFRP correspondingly
A_s, A_{res}, A_{cfrp} are the cross-section areas of steel, resin or CFRP correspondingly
E_s, E_{res}, E_{cfrp} are the moduli of elasticity of steel, resin or CFRP correspondingly
$n_{res} = E_s/E_{res}$ is the modular ratio of the resin
$n_{cfrp} = E_s/E_{cfrp}$ is the modular ratio of the CFRP

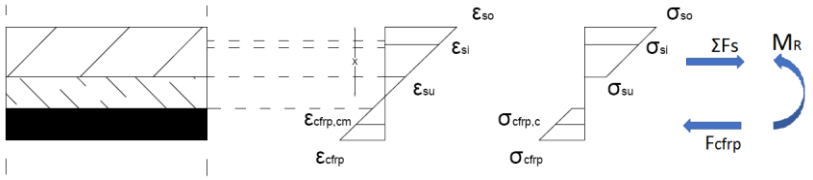

Figure 17: Calculation procedure for the internal moment – Analytical method 1

Starting from the strains as measured during the test, the internal moment is determined by the strip method as indicated in Fig. 17 neglecting the contribution of the resin. The analytical moment – deflection curve is illustrated in Fig. 18 and compared with the experimental one. The disadvantage of the analytical method 1 is that no experimental strain data are available at the late loading steps so that the moment can be calculated up to a certain point (up to a deflection 25 mm in Fig. 18).

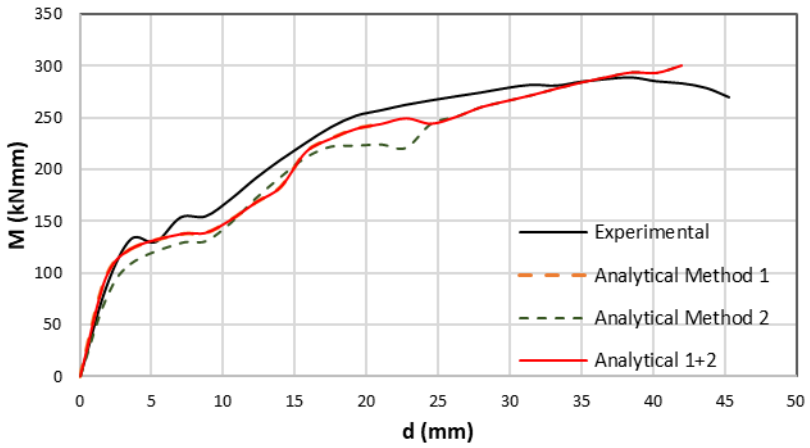

Figure 18: Experimental and analytical moment – deflection curves

- Analytical Method 2

In this method the computation process is reversed. The tension force in the CFRP, acting at its centroid, is determined from eq. (12):

$$F_{cfrp} = E_{cfrp} \cdot \varepsilon_{cfrp} \cdot A_{cfrp} \quad (12)$$

where:

ε_{cfrp} is the strain at the CFRP centroid of the CFRP. It is taken as ½ of the measured CFRP strain, since the plastic neutral axis of the composite section is considered to be within the adhesive.

The tension force in the CFRP is equal for equilibrium reasons to the compression force in steel, Fig. 19. The stress distribution in steel is assumed uniform across its thickness. The steel stress is determined from measurements as long as strain data for steel are available. After it, the steel stresses are estimated under consideration of strain hardening. The so calculated moments are shown in Fig. 18.

It may be seen that despite the missing strain measurements, method 2 is appropriate for the late loading steps at large strains where steel is yielding and strain hardening, while method 1 fits better for the early loading steps. Fig 18 shows that the combination of the two methods may provide a good estimate of the specimen's response.

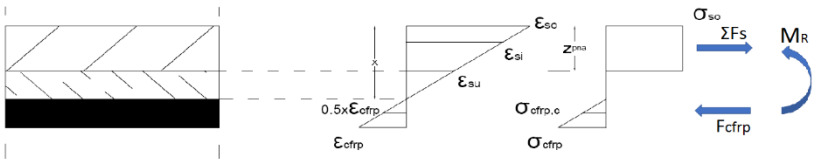

Figure 19: Calculation procedure for the internal moment – Analytical method 2

The bending test was also investigated numerically with the same modelling using the ABAQUS Code as previously described. Fig. 20 shows the test specimen in its deformed shape, together with the corresponding numerical model.

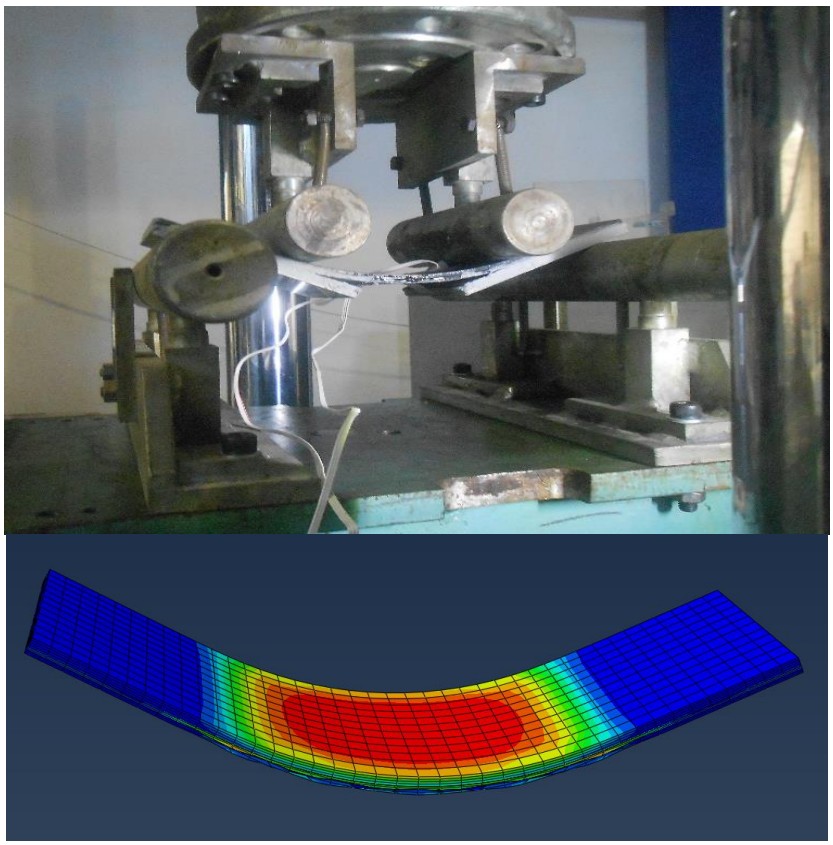

Figure 20: Experimental and numerical model at its deformed state

The calculations included MNA and GMNA analyses, where in the former only the material non-linearity and in the latter the geometric and material non-linearity were considered. Fig 21 shows the experimental and numerical results. It may be seen that the numerical results fit well with the experimental ones, especially when the effects of slip are removed from the experimental ones. The numerical models, especially the GMNA analysis, predict a smaller capacity due to the neglect of any contribution of the adhesive. However, the initial stiffness is very close to the experimental one.

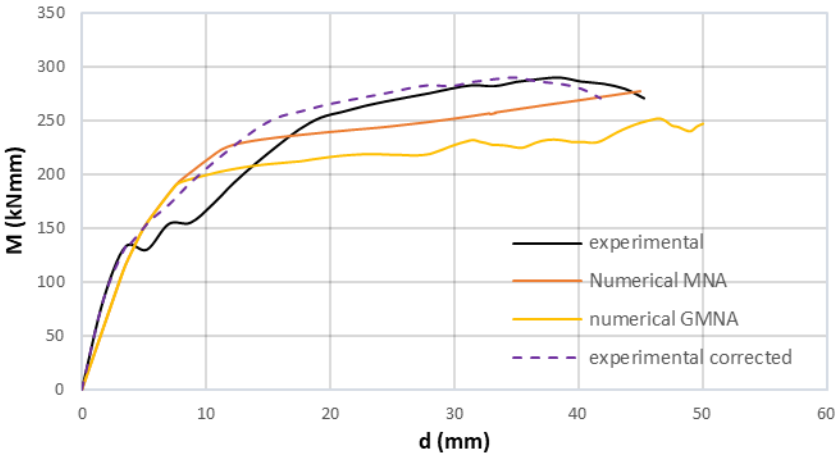

Figure 21: Experimental and numerical moment – deflection curves

5 FOUR-POINT BENDING TEST – FRP ON THE COMPRESSION SIDE

The test set-up, the measurements and all other data are the same as before, except that the specimen is put upside down, so that the CFRP is on the compression side, Fig. 22. For the same reasons as before, at late loading stages no CFRP strain data were available because the strain gauge was disconnected at the compression side due to very high strains.

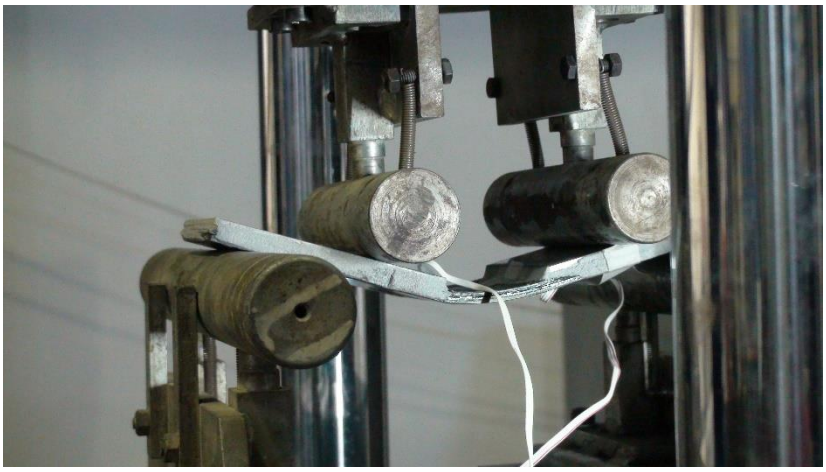

Figure 22: Test set-up for the 4-point bending test – CFRP in compression

Fig. 23 shows the experimental and analytical moment – deflection curves. The analytical curves were determined by the two methods described before. It may be seen that the combination of methods 1 and 2 provides acceptable results, even if the contribution of the resin

was neglected. Based on the analytical calculations, the compression strength of the CFRP is estimated to be 640 MPa.

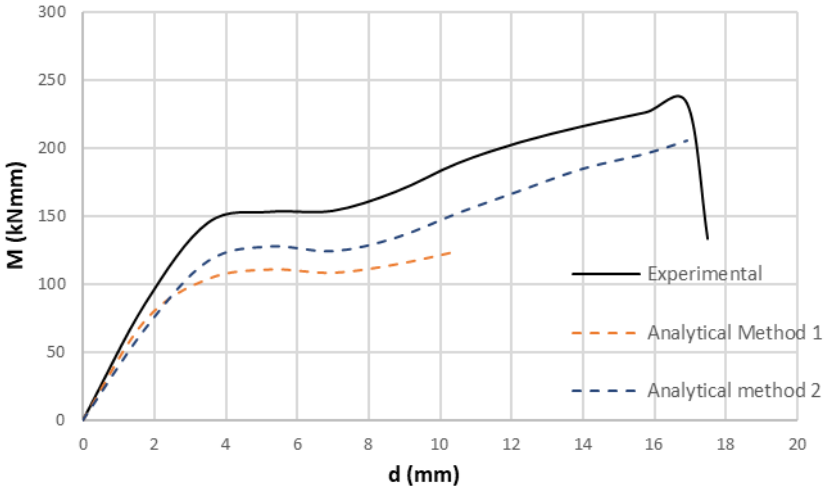

Figure 23: Experimental and analytical moment – deflection curves

This test was also studied numerically using the same model as in the other tests. Especially, the material properties of the CFRP were taken as those for tension. Both MNA and GMNA analyses were performed. The deformed shape of the model for the GMNA analysis is shown in Fig. 24 and may be compared to the deformed shape of the experimental model shown in Fig. 22.

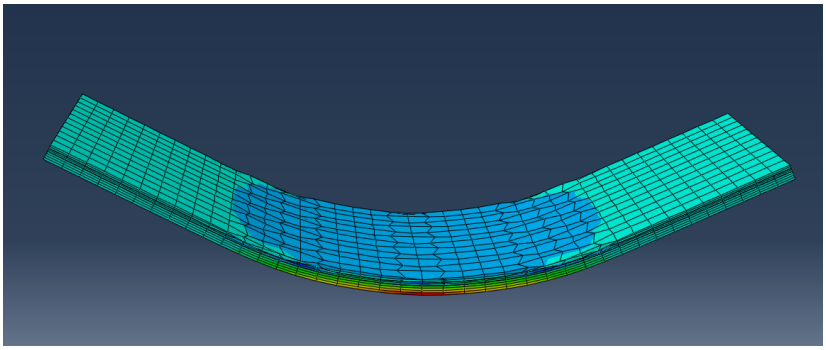

Figure 24: Deformed shape of the numerical model by GMNA analysis

Fig. 25 shows the experimental and numerical moment - deflection curves. It may be seen that for this test the GMNA analysis provides better results. However, the numerical analyses cannot predict the moment capacity due to the fact that for the CFRP material the linear elastic tension properties were introduced. Accordingly, the large deflections predicted numerically are not realistic if the tension properties of the material are adopted. Based on the stresses of the numerical model at the maximal deflections of the experiment, the compression strength of the CFRP is estimated as 700 MPa, which is similar to 640 MPa as determined with the analytical model. This is around 30% of the nominal tension strength. However, it should be noted that no local buckling occurred in this test.

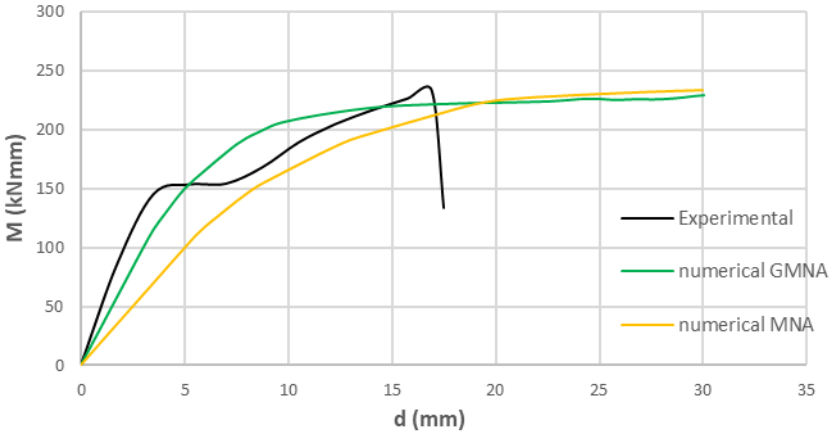

Figure 25: Experimental and analytical moment – deflection curves

The numerical model was further on used to calculate the 4-point bending response of the steel plate alone without any CFRP strengthening. Fig. 26 compares the derived curve in comparison with the experimental curves of the same steel plate strengthened with CFRP on the tension or the compression side. It may be seen that the bending capacity of the steel plate increased almost 6 times by strengthening it with CFRP in the tension side. When the CFRP was placed on the compression side this increase was less, around 4.6 times, confirming the lower strength of CFRP when it is used for compression. However, the stiffness of the strengthened specimens was equal indicating that the same modulus of elasticity may be used for the CFRP either in compression or tension. Important is that the ductility of the composite specimen is exhausted when the CFRP material is reaching its compression capacity.

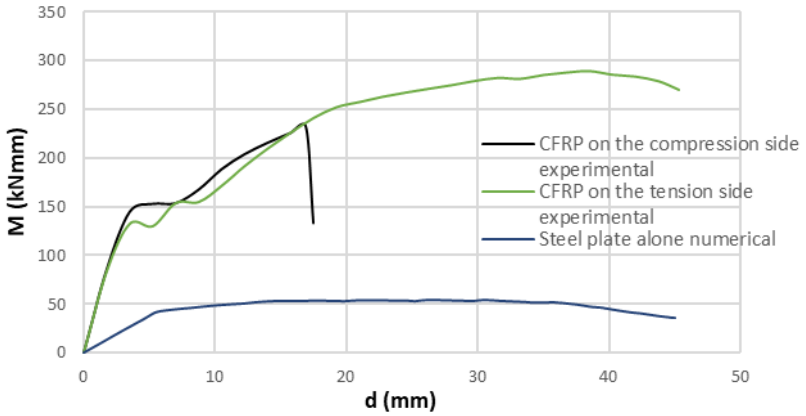

Figure 26: Moment – deflection curves for steel plates with and without CFRP reinforcement subjected to 4-point bending

6 CONCLUSIONS

The behavior of steel plates reinforced in one side with carbon fiber reinforced polymer (CFRP) has been studied experimentally, analytically and numerically. The properties of the source material have been determined experimentally. Subsequently, the composite material has been subjected to tension tests and four-point bending tests with the reinforcement on the tension and the compression side. The test material has been prepared in BTU Cottbus, Germany, while the tests have been executed in NTUA, Athens, Greece. Analytical relations have been derived on the basis of the Bernoulli assumption of linear strain distribution in the cross

section and numerical investigations with application of the FEM have been performed. From the studies carried out following conclusions may be drawn:

1. One-sided strengthened steel plates subjected to axial tension forces exhibit permanent bow deformations after unloading due to irreversible plastic deformations of steel.
2. Existing analytical relations for defining the properties of the CFRP plates in relation to the properties of the two constituent materials, the carbon fibers and the matrix, have been confirmed.
3. The modulus of elasticity of CFRP was equal, whether the CFRP was in the tension or in the compression side.
4. The strength of the CFRP was different for compression and tension, the former being a fraction of the latter.
5. The assumption of a composite section from two different materials, the Bernoulli assumption of linear strain distribution in the cross-section and the assumption of no slip between the two constituent materials are valid for this type of strengthening, provided that appropriate adhesives are used and their application follows the relevant specifications for their connection.
6. Design for CFRP strengthening of steel elements where the CFRP is in the tension side may be based on the nominal material properties of CFRP as determined by the specified tensile testing.
7. For CFRP strengthening of steel elements where the CFRP is in the compression side, only the modulus of elasticity of CFRP as determined by the tensile testing may be used, while its strength must be reduced
8. Four-point bending tests of the composite material with no local buckling as outlined here, where the CFRP is in the compression side are appropriate to define the properties of the CFRP material to compression.

ACKNOWLEDGEMENTS

The financial support of the Deutscher Akademischer Austauschdienst (DAAD) through the project “Verstärkungsmaßnahmen und innovative Messmethoden im Stahlbau“ and of the Research Fund of Coal and Steel (RFCS) through the project ANGELHY is gratefully acknowledged.

REFERENCES

[1] FRP EBR (2001), Design and use of externally bonded FRP reinforcement, FIP

[2] EN 1998-3 (2005). Eurocode 8. Earthquake resistant design of structures. Part 3 Assessment and retrofitting of buildings, European Committee for Standardization (CEN), Brussels, Belgium.

[3] ACI 440.2R-02 (2002), “Guide for the Design and Construction of Externally Bonded FRP Systems for Strengthening Concrete Structures”, American Concrete Institute

[4] National Cooperative Highway Research Program NCHRP Report 514 (2004), “Bonded Repair and Retrofit of Concrete Structures Using FRP Composites”

[5] Teng JG, Yu T, Fernando D (2012). Strengthening of steel structures with fiber-reinforced polymer composites, J. of Constructional Steel Research, Elsevier, 78, 131-143.

[6] Al-Saidy AH, Klaiber FW, Wipf TJ (2004), Repair of steel composite beams with carbon fiber-reinforced polymer plates, J. of Composites for Construction (ASCE), 8(2), 163-172

[7] Miller TC, Chajes MJ, Mertz DR, Hastings JN (2001), Strengthening of a steel bridge girder using CFRP plates, J. of Bridge Engineering (ASCE), 6(6), 514-522

[8] Silvestre N, Young B, Camotim D (2008) Non-linear behavior and load-carrying capacity of CFRP -strengthened lipped channel steel columns, Engineering Structures, 30, 2613-2630

[9] Bassetti A, Nussbauer A, Colombi P (2000), Repair of riveted members damaged by fatigue using CFRP materials, Advanced FRP Materials for Civil Structures, Bologna, Italy, 19th October, 33-42

[10] Haedir J, Zhao XL (2011), Design of short CFRP-reinforced steel tubular columns, J. of Constructional Steel Research, Elsevier, 67, 497-509

[11] Hu YM, Yu T, Teng JG (2011), FRP-confined circular concrete-filled thin steel tubes under axial compression, J. of Composite Construction (ASCE), 15(5), 850-860

[12] CNR-DT 202 (2005), "Guidelines for the Design and Construction of Externally Bonded FRP Systems for Strengthening Existing Structures – Metallic Structures", CNR, Rome, 2007

[13] EU DG Research and Innovation, Grant agreement 753993 – ANGELHY, 2017

[14] Deutscher Akademischer Austauschdienst (DAAD), Project 57339810, Verstärkungsmaßnahmen und innovative Messmethoden im Stahlbau, 2017

[15] ISO 527-1 (2012). Plastics: "General principles for determination of tensile properties"

[16] ISO 527-4 (1997). Plastics: "Test conditions for isotropic and orthotropic fiber-reinforced plastic composites"

[17] ASTM D638 – 03 (2003) "Standard Test Method for Tensile Properties of Plastics"

[18] ASTM D3039/D3039M – 17 (2017). "Standard Test Method for Tensile Properties of Polymer Matrix Composite Materials"

[19] Vlachaki-Karagiannopoulou S (2018) Behavior of fiber reinforced polymers with experimental and analytical methods, MSc-Thesis, NTUA

[20] Vlachakis K (2018) Analysis and design of a telecommunication steel tower strengthened with FRP plates, MSc-Thesis, NTUA

[21] EN ISO 6892-1 (2009), "Metallic materials - Tensile testing: Method of test at room temperature"

[22] ABAQUS (2008). *ABAQUS User's Manual*. Version 6.14, Dassault Systems Simulia Corp., Providence, RI, USA

[23] Pederson J (2008). Finite Element Analysis of Carbon Fiber Composite Ripping using Abaqus, All Theses, Paper 512, Clemson University, Clemson, SC